The influence of Al doping on the photocatalytic activity of nanostructured ZnO: the role of adsorbed water

Faten Ajala[1] , Abdessalem Hamrouni[1], Ammar Houas[1,2], Hinda Lachheb[1], Bartolomeo Megna[3], Leonardo Palmisano*[4], Francesco Parrino*[4]

[1] *Unité de Recherche Catalyse et Matériaux pour l'Environnement et les Procédés URCMEP (UR11ES85); Faculté des Sciences de Gabès / Université de Gabès; Campus Universitaire -Cité Erriadh- 6072 Gabès, Tunisie.*

[2] *Al Imam Mohammad Ibn Saud Islamic University (IMSIU), College of Sciences, Department of Chemistry, Riyadh 11623, Saudi Arabia.*

[3] *Dipartimento di Ingegneria Civile, Ambientale, Aerospaziale e dei Materiali (DICAM), University of Palermo, Viale delle Scienze Ed. 6, Palermo 90128, Italy.*

[4] *Dipartimento di Energia, Ingegneria dell'Informazione e Modelli Matematici (DEIM), University of Palermo, Viale delle Scienze Ed. 6, Palermo 90128, Italy.*

corresponding authors: francesco.parrino@unipa.it; leonardo.palmisano@unipa.it

Abstract

Al doped ZnO nanoparticles (labeled as x% A-ZnO, x = 0.0, 0.5, 1.0, and 1.5) were synthesized by a simple sol-gel method, characterized and tested as photocatalysts for the degradation of a model compound under UV-light irradiation. Diffuse reflectance spectroscopy (DRS) and photoelectrochemical analysis have been performed to evidence their optical and electronic behavior. The structural features of the powders were highlighted by means of specific surface area (SSA) analysis, X-ray diffraction (XRD), Fourier-transform infrared (FTIR) and Raman spectroscopy. Al doping results in enhanced photocatalytic activity of the modified powders with respect to pure ZnO. In particular, the highest activity was achieved with the 1.0% A-ZnO sample. The presence of Al did not significantly change neither the optical absorption nor the electronic structure of the powders. In fact, the observed blue shift of the band gap and cathodic shift of the quasi Fermi level of the modified powders occurred only at a virtually negligible extent. On the other hand, the structural analysis evidenced that the enhanced photocatalytic activity may be ascribed to the important surface defectivity induced mainly by substitution of Zn^{2+} by Al^{3+} ions and to the deriving higher hydrophilicity of the Al doped samples.

Keywords: Al-doped ZnO, sol-gel, nanoparticles, photocatalysis, defects, adsorbed water, ZnO

1. Introduction

Heterogeneous photocatalysis is nowadays one of the most promising tools for a future sustainable development. In fact, the possibility of exploiting clean and renewable solar light harvested by cheap, abundant and non toxic metal oxides is highly appealing in view of the environmental and energetic challenges of the future [1]. The versatility of photocatalysis is a matter of fact by taking into account its manifold applications in the field of environmental remediation in gas [2] and liquid phase [3], disinfection [4], self-cleaning surfaces [5], green synthesis [6], energy [7], and solar cells [8]. Due to the wide range of different applications the scientific community addressed many efforts in tailoring and opportunely modifying the properties of promising materials such as titanium dioxide (TiO_2) and zinc oxide (ZnO). In particular, both surface and bulk modifications have been performed in order to extend their light absorption ability from UV to visible range [9], to enhance their affinity with target chemical compounds in organic synthesis [10], or to endow them with desired physico-chemical properties [11].

Metal doping is one of the most used techniques to these aims. Noble metals such as silver, gold, rhodium or platinum have been deposited on the surface of TiO_2 or ZnO in the form of metal nanoparticles [12], or chemically bonded in other oxidation states [13], giving rise to visible light activity of the powders or selectively addressing target chemical reactions such as hydrogen generation or organic synthesis.

Insertion of metal ions into the lattice of semiconductors is another technique to induce defectivity and confer specific properties to the material [14]. This modification has been mainly used to induce bulk properties such as high electric and thermal conductivity, which are essential features for applications in thermoelectric devices able to convert heat in electricity and vice versa [15]. Notably, the defectivity induced by bulk modifications is of paramount importance also for photo- and catalytic applications and is still object of scientific debate [16]. Among the wide range of metals used for bulk modifications of ZnO, aluminum is a paradigmatic case. In fact, while Al doped ZnO is one of the best and most studied n-type material for thermoelectric applications reported to date [17], only relatively few papers investigated the reasons for its enhanced photocatalytic activity and in most cases different experimental evidences and controversial interpretations are reported.

Different preparation methods such as coprecipitation [18], spray pyrolysis [19], sol-gel [20], hydrothermal routes [21], pulsed-laser deposition [22], and combustion [23] have been used. Some papers focus on the optical features of Al modified ZnO, indicating them as the key

factors for the improved photocatalytic activity. Ahmad et al. [23] reported that doping ZnO with Al extended the light absorption edge of the oxide to the visible range (red shift) thus improving the photocatalytic degradation of methyl orange. On the other hand, Alkahlout et al. [21] reported that Al doped ZnO nanoparticles presented a blue shift of the band gap with respect to the starting material. Similar results were obtained for Al doped ZnO thin films [24-25]. Conversely, Lee et al. [26] reported that the band gap of ZnO is virtually not influenced by the presence of Al (up to 8 mol%) and attributed the enhanced methyl orange photocatalytic degradation rate to a vaguely invoked reduced electron-hole recombination. Pal et al. [20] ascribed the enhanced rhodamine B photocatalytic oxidation in the presence of Al doped ZnO thin films to the presence of defectivity and reported a blue shift of the doped materials with respect to the pristine ZnO.

The present investigation aims to clarify the features responsible for the enhanced photocatalytic activity by means of a thorough characterization of Al doped ZnO nanoparticles prepared by a simple sol-gel method. In particular, the electronic map of the materials has been obtained by combining an optical analysis (diffuse reflectance spectroscopy) with a potentiometric titration method in aqueous suspension strongly mimicking the real photocatalytic experimental conditions. Furthermore, the structural defects induced by Al doping have been evidenced by means of XRD, FTIR and Raman spectroscopy. A comparative analyses of the data showed that the electronic features of the samples are of minor importance, while the structural modifications and the induced surface hydrophilicity are mainly responsible for the enhanced photocatalytic activity.

2. Material and methods

2.1. Synthesis of Al doped ZnO photocatalysts

Zinc acetate dihydrate ($Zn(CH_3COO)_2 \cdot 2H_2O$ reagent grade, Sigma Aldrich) and aluminum sulfate octadecahydrate ($Al_2(SO_4)_3 \cdot 18H_2O$ reagent grade, Sigma Aldrich), methanol (CH_3OH p.a., Sigma Aldrich), ammonium hydroxide solution (NH_4OH 28%, Fluka), and Indigo Carmine (p.a. Sigma-Aldrich) were used as received without further purification.

A 0.1 M methanol solution of zinc acetate dihydrate was stirred at 70°C and added to a methanol solution of aluminum sulfate octadecahydrate. The concentration of the aluminum sulfate solution was fixed to obtain samples with Al/Zn molar ratio equals to 0.005/1, 0.01/1, and 0.015/1 which were labeled as 0.5%A-ZnO, 1.0%A-ZnO and 1.5%A-ZnO, respectively. The obtained solution was continuously stirred for 2 hours at 70°C. Then, the ammonia solution was added dropwise until pH 7. The resulting gel was dried for 24 hours at 110°C to give a xerogel. The latter was calcined for 2 hours at different temperatures (500, 600 and 700 °C) and eventually cooled down and ground. The pure ZnO sample was analogously synthesized but using only the zinc acetate solution.

2.2. Characterization of the samples

XRD analysis was performed by using an Italstructures APD 2000 powder diffractometer with Cu Kα radiation source. The mean particle size (D) was calculated by the Debye–Scherrer formula:

$$D = 0.9 \lambda / \beta \cos\theta \quad (1)$$

where λ is the wavelength of the X-ray radiation (0.154 nm), θ is the diffraction angle and β is the corrected full width at half maximum height. The lattice parameters were calculated through the software FullProf using the standard method.

The specific surface area (SSA) was determined by the single point Brunauer Emmet Teller (BET) method using a Micromeritics Flowsorb 2300 instrument.

Diffuse reflectance spectra were recorded by means of a Shimadzu UV-2401PC spectrophotometer. Barium sulfate ($BaSO_4$) was used as a reference and the analysis was performed in the range of 200–800 nm. The values of the band gap energy (E_g) were determined by using the Kubelka-Munk transformed and extrapolating the linear part of the Tauc plot $(F(R'_\infty) \cdot h\nu)^2$ vs $(h\nu)$.

Infrared (FTIR) spectroscopy was performed by using a Shimadzu FTIR-8400S by dispersing the samples in KBr and analyzing the pellet obtained by using a hydraulic press.

Raman spectra were obtained by means of a BWTek-i-micro Raman Plus System, equipped with a 785 nm diode laser. The power of the laser was 15% of the maximum value (about 300 mW). The measurements were performed focusing the sample by a 5x magnification lens. The accuracy of the Raman shift was approximately 3 cm^{-1}.

2.3. Photovoltage measurements

A Pyrex reactor with a total volume of 150 mL was used for the determination of the quasi-Fermi level of the samples. 100 mg of the photocatalyst were added to 100 mL of a 0.1 M sodium nitrate ($NaNO_3$) solution. Platinum (Pt) and Ag/AgCl electrodes were employed as working and reference electrodes, respectively. The suspension was kept under irradiation and N_2 was bubbled through it for 30 minutes. Thereafter 20 mg of methyl viologen (1,1'-dimethyl-4,4'-bipyridinium dichloride) were added to the suspension and nitrogen bubbling was maintained further for 30 minutes before starting the potentiometric titration. The pH of the solution was adjusted by adding nitric acid (HNO_3) and sodium hydroxide (NaOH) solutions and the values of pH and the potential (V) were measured by using a pH meter Thermo Orion 720A and a multimeter Mets 3800, respectively. The suspension was irradiated during the measurement by two medium pressure Hg UV lamps (Philips HPK 125 W).

2.4. Photocatalytic experiments

The photocatalytic activity of the samples was estimated by monitoring the degradation of Indigo Carmine (IC) as the model compound. A cylindrical Pyrex photoreactor, containing 30 ml of the IC aqueous solution ($4 \cdot 10^{-2}$ $g \cdot L^{-1}$) and 1 $g \cdot L^{-1}$ of the photocatalyst, was used to carry out the photodegradation experiments. Six medium pressure Hg lamps (8 W each) were axially positioned around the photoreactor at a distance of 7 cm from its external surface. The amount of catalyst was chosen in order to ensure that almost all of the photons entering the reactor were absorbed by the reacting suspension. In this way the results of runs carried out in the presence of different photocatalysts could be compared [27]. The reactor was cooled down through water circulating in a Pyrex thimble. The reaction mixture was mechanically stirred for 120 minutes in the dark prior to irradiation to attain the adsorption-desorption equilibrium of the substrate. Samples were taken at different time

intervals, filtered through a 0.2 µm filter and analyzed by means of a UV-vis Shimadzu UV-2401PC spectrophotometer in order to evaluate the extent of IC degradation.

3. Results and discussion

3.1. Photocatalytic activity results

Figure 1 shows the degradation of IC during irradiation in the presence of photocatalysts with different aluminum contents calcined at 600 °C (Figure 1 A) and in the presence of 1.0%A-ZnO calcined at 500, 600 and 700 °C for 2 hours (Figure 1 B).

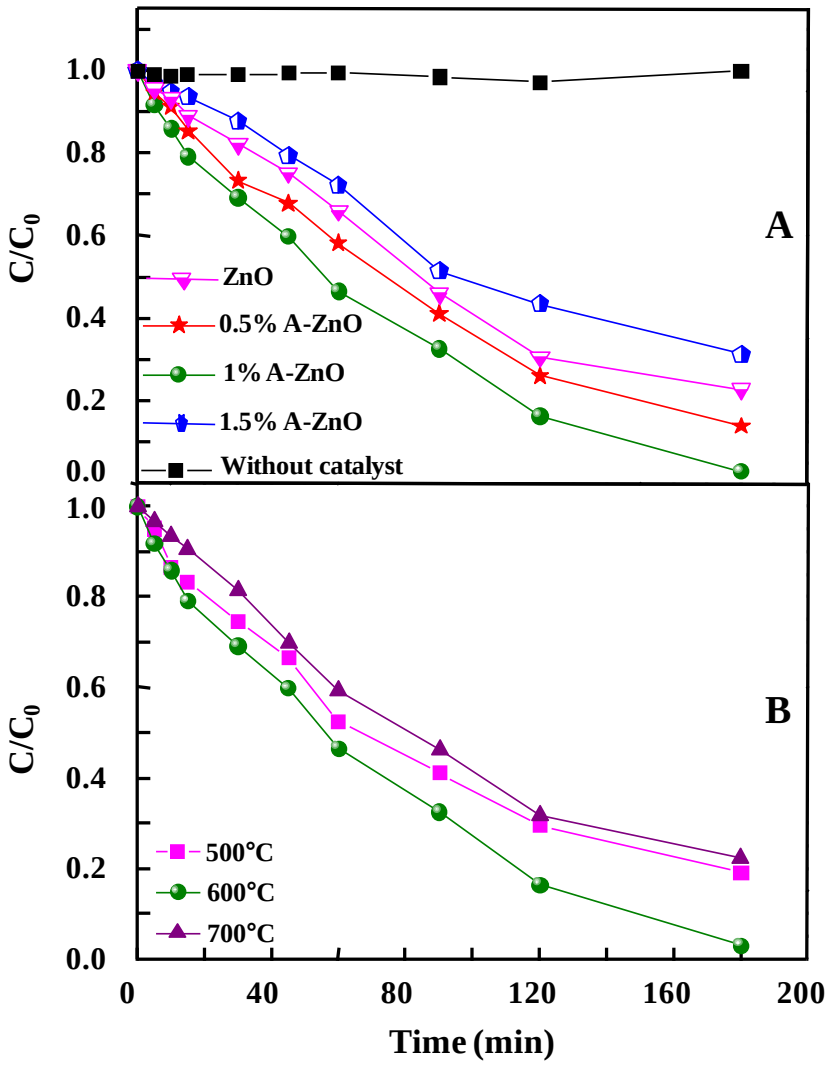

Figure 1. Degradation of IC ($4 \cdot 10^{-2}$ g·L^{-1}) under UV light in the presence of Al doped ZnO photocatalysts (1 g·L^{-1}): (A) in the absence of photocatalyst (black squares), and in the presence of x% A-ZnO calcined at 600 °C for 2h, x = 0 (pink triangles), 0.5 (red stars), 1.0 (green circles), and 1.5 (blue pentagons); (B) IC photodegradation in the presence of 1.0% A-ZnO calcined at 500 °C (pink squares), 600 °C (green circles) and 700 °C (purple triangles).

IC concentration was stable under irradiation in the absence of the photocatalyst thus indicating that the photolytic mechanism may be safely neglected. Furthermore, IC concentration did not change in the presence of the photocatalyst but under visible light irradiation. This suggests that, although IC excitation occurs under visible light, electrons did not transfer from the IC excited state to the conduction band of ZnO. Therefore, the use of a dye as the model compound is justified, being the excitation of the photocatalyst responsible for the UV light activity, while the indirect photocatalytic mechanism does not play a significant role in the present experimental conditions [28-29].

Under UV light irradiation IC degradation occurred in the presence of all of the considered photocatalysts. In particular, after 3 hours 68, 86, 97 and 77% of the initial IC concentration were consumed over ZnO, 0.5% A-ZnO, 1.0% A-ZnO and 1.5% A-ZnO, respectively. Therefore, the photocatalytic activity increased with increasing Al content reaching a maximum for the 1.0% A-ZnO sample and then decreased at higher Al concentrations, being for the 1.5% A-ZnO sample even less than for the bare ZnO. Similar behavior is reported for other ZnO based systems [30-33].

Figure 1 B shows the influence of the calcination temperature on the photocatalytic activity. Calcining at temperatures lower than 500 °C did not ensure a homogeneous composition of the powders, so that the photocatalytic activity was studied for powders calcined in the range 500-700 °C. The highest photocatalytic activity was obtained by calcining the sample at 600 °C. The values of the apparent kinetic constant (k_{app}) were obtained from the plot of ln (C_0/C) versus time (C_0 and C were the initial and the actual concentrations, respectively). Only the first 15 min of the reaction were considered. Results ranged from $4 \cdot 10^{-3}$ and $15 \cdot 10^{-3}$ min^{-1} and are summarized in Table 1.

Table 1. The apparent kinetic constants (k_{app}) of the degradation of IC.

	ZnO 600°C	0.5%A-ZnO 600°C	1.0%A-ZnO 600°C	1.5%A-ZnO 600°C	1.0%A-ZnO 500°C	1.0%A-ZnO 700°C
k_{app} ($10^{-3}min^{-1}$)	4	10	15	6	12	6

Figure 2 shows the IC adsorption ability of bare and Al doped ZnO samples during time in the dark.

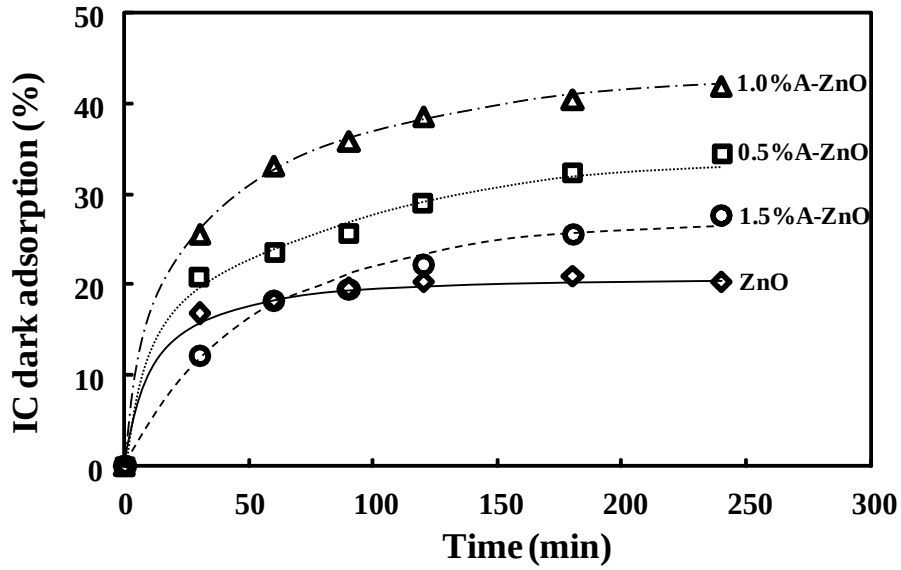

Figure 2. Percentage of IC adsorbed in the dark on ZnO (rhombi, solid line), 0.5% A-ZnO (squares, dotted line), 1.0% A-ZnO (triangles, dotted-dashed line), and 1.5% A-ZnO (circles, dashed line) photocatalysts calcined at 600 °C. Initial IC concentration: $4 \cdot 10^{-2}$ g·L^{-1}. Catalyst load: 1 g·L^{-1}.

Bare ZnO reached the adsorption-desorption equilibrium faster than the other samples. However, the amount of IC adsorbed under equilibrium conditions was higher for the Al doped samples with respect to ZnO. In particular, among the modified powders, 1.0% A-ZnO sample showed the highest adsorption ability while the 1.5% A-ZnO one the lowest. Notably, samples with higher IC adsorption ability in the dark showed higher photocatalytic activity.

In order to unravel the reasons of the enhanced photocatalytic activity and adsorption in the dark of the Al doped samples with respect to bare ZnO, the below reported opto-electronic and structural characterizations have been performed.

3.2 Opto-electronic characterization

The optical properties of the photocatalysts were investigated through DRS at room temperature. The Tauc plots of bare ZnO and Al doped samples are presented in Figure 3 along with the indication of the band gap energy. The inset shows the diffuse reflectance spectra of the sample 1.0% A-ZnO calcined at different temperatures for 2h.

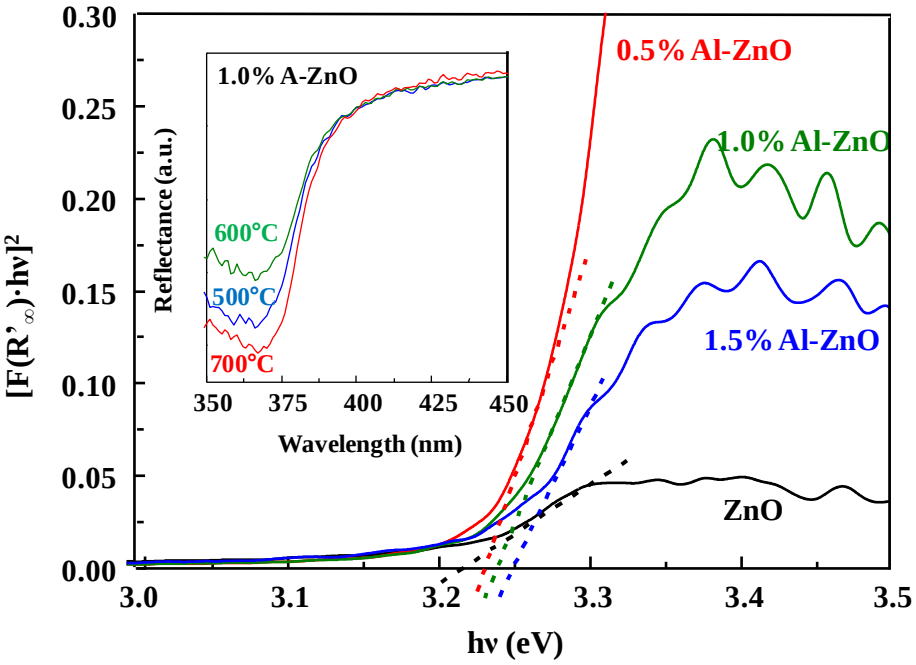

Figure 3. Tauc plots of ZnO (black line), 0.5% A-ZnO (red line), 1.0% A-ZnO (green line), and 1.5% A-ZnO (blue line), obtained by considering the samples direct semiconductors. Inset: Diffuse reflectance spectra of 1.0% A-ZnO sample calcined at 500 (blue line), 600 (green line) and 700 °C (red line).

The band gap energy of ZnO is 3.21 eV in agreement with the relevant literature [30-33]. Increasing the Al content in the powders results in a slight blue shift of the absorption edge. Indeed the band gap energy is 3.23, 3.24, and 3.25 for 0.5%A-ZnO, 1.0% A-ZnO, and 1.5% A-ZnO, respectively. Notably, the temperature did not have significant influence on the band gap energy, as shown in the inset of Figure 3.

The quasi-Fermi level of electrons for the considered photocatalysts was determined experimentally by using the potentiometric method reported by Roy et al. [34] carried out in irradiated aqueous suspensions of the photocatalysts. This method gives information on the potential of the photogenerated electrons in a system strongly mimicking the actual

photocatalytic reaction conditions, and is therefore very helpful for the present investigation. Figure 4 shows the plot of the photovoltage versus pH in the presence of bare ZnO and the Al doped photocatalysts.

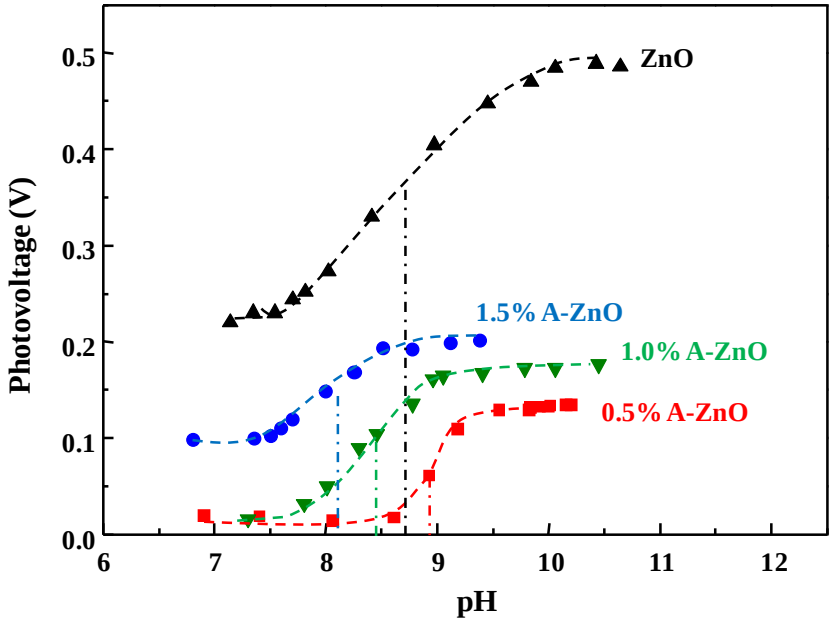

Figure 4. Photovoltage vs. pH titration curves of pure ZnO and of the Al doped ZnO samples. Each titration was repeated at least three times.

The potential of the flat band was determined at pH 7 using the following relation:

$$E_{FB(pH=7)} = E^0_{MV^{2+}/MV^{+\bullet}} + 0.059\ (pH_0 - 7) \qquad (2)$$

where the standard potential of the $MV^{2+}/MV^{+\bullet}$ couple ($E^0_{MV^{2+}/MV^{+\bullet}}$) is equal to − 0.45 V vs. NHE [35]. The pH at the inflection point of the sigmoidal titration curves (pH_0, indicated in Figure 4 by a dashed-dotted line) is experimentally evidenced by the blue color originated from the formation of the reduced form of methyl viologen. In fact, at pH = pH_0 the E_{FB} reaches $E^0_{MV^{2+}/MV^{+\bullet}}$ and electrons transfer from the photocatalyst to reduce MV^{2+} ions. The pH_0 and E_{FB} values of the powders, are reported in Table 2 along with the band gap energies (E_g) obtained through the optical analysis (DRS).

Table 2. Inflection point of the titration curves (pH_0), quasi-Fermi level of electrons (E_{FB}), and band gap energies (E_g) of pure ZnO and of x% A-ZnO (x = 0.5, 1.0, and 1.5). Reproducibility was better than ± 0.02 V.

	pH_0	**E_{FB} (V)**	**E_g (eV)**
ZnO	8.7	-0.35	3.21
0.5% A-ZnO	8.8	-0.34	3.23
1.0% A-ZnO	8.5	-0.36	3.24
1.5% A-ZnO	8.2	-0.38	3.25

By taking into account the experimental error, one can conclude that both the E_{FB} and E_g values obtained are quite similar for all of the photocatalysts. Nevertheless, it is possible to observe that increasing the Al content results in a cathodic shift of the E_{FB} values and in a blue shift of the band gap energies, i.e the Fermi level moves towards more negative potential values and the band gap energy increases. This finding may be explained by considering the Al doping mechanism summarized in Eq. 3 [36].

$$\infty ZnO + 2Al^{3+} + 3O^{2-} \rightarrow 2Al^{+} + \infty ZnO + \tfrac{1}{2} O_2 + 2e^{-} \quad (3)$$

Substitution of Zn^{2+} with Al^{3+} ions provokes the release of oxygen which leaves its electrons in the matrix. Therefore, the system presents higher electron concentration [37] and increases its n-type character with respect to the pristine ZnO. As a consequence, while generally the Fermi level of ZnO lies closely below the conduction band, in the presence of Al the electrons generated by Eq. 3 populate states within the conduction band so that the Fermi level moves towards higher energy values. Since all of the states below the Fermi level are forbidden according to the Pauli's exclusion principle, electrons can only be excited from the valence band to the states above the Fermi level (which now lies in conduction band). This occurrence, known as the Burstein-Moss effect [38], justifies the enhanced conductivity of these samples with respect to ZnO reported in literature [39] and explains the hereby observed opto-electronic behavior of the Al-doped samples. Interestingly, Shinde et al. [22] reported that a similar blue shift observed in pulsed-laser deposited Al doped ZnO thin films disappeared upon annealing of the samples at 800 °C.

However, such small variations in the electronic features of the powders cannot be invoked to explain the enhanced photocatalytic activity above discussed. Therefore, we proceeded investigating the defectivity induced by the presence of Al in the ZnO matrix.

3.3 Structural analysis

The substitution of Zn^{2+} with Al^{3+} ions summarized by Eq. 3 and hypothesized to justify the opto-electronic features of the powders has been validated by characterizing the structural changes in the lattice of ZnO and the induced defectivity. These factors have been investigated by means of XRD analysis, FTIR and Raman spectroscopy.

3.3.1 XRD analysis

Figure 5 shows the XRD patterns of the powders calcined at 600 °C (A) and of the 1.0% A-ZnO sample calcined at 500, 600, and 700 °C.

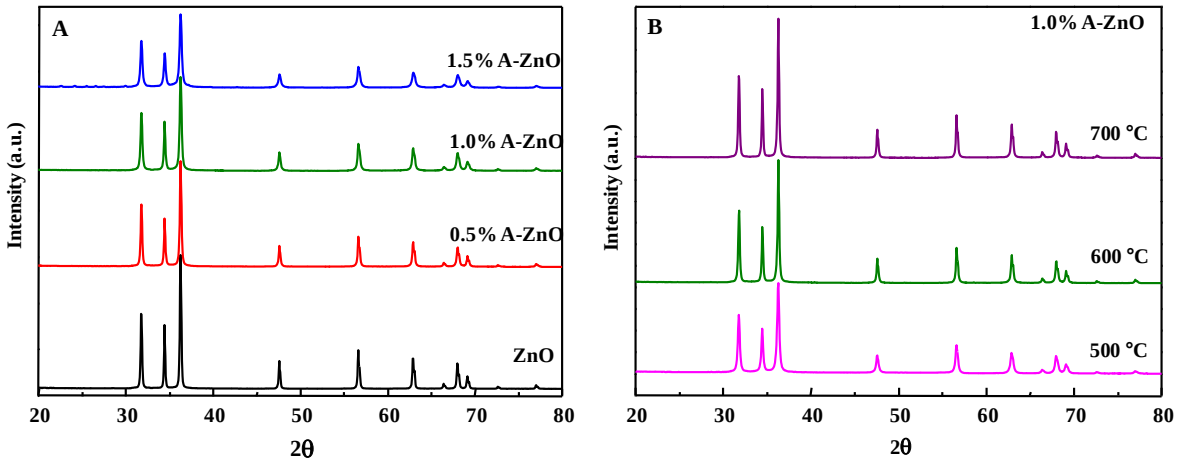

Figure 5. XRD patterns of ZnO and of x% A-ZnO (x = 0.5, 1.0, and 1.5) powders calcined at 600 °C (A) and of 1.0%A-ZnO sample calcined at different temperatures (B).

The mean grain size of the particles was determined by applying the Debye-Scherer formula on the (101) diffraction peak of ZnO. Values are reported in Table 3 along with the specific surface area (SSA) of the samples obtained by means of single point Brunauer Emmet Teller (BET) analysis.

Table 3. Specific surface area (SSA) and mean particle size of ZnO and x% A-ZnO (x = 0.5, 1.0, 1.5) powders calcined at 600 °C and of 1.0% A-ZnO sample calcined at different temperatures.

	ZnO 600°C	**0.5% A-ZnO 600°C**	**1.0% A-ZnO 600°C**	**1.5% A-ZnO 600°C**	**1.0% A-ZnO 500°C**	**1.0% A-ZnO 700°C**
SSA ($m^2 \cdot g^{-1}$)	4	8	9	11	16	6
Mean particle size (nm)	53	49	49	47	38	51

The patterns in Figure 5 may be ascribed to ZnO hexagonal wurtzite structure (JCPDS card No. 36-1451). All of the samples show high purity and no diffraction peaks relative to aluminum secondary phases such as spinels, Al_2O_3 or any impurities can be observed. Accordingly, Tsubota et al. [40] reported formation of spinel secondary phases like $ZnAl_2O_4$ for Al contents relative to Zn higher than 5%. Notably, Hong et al. [41] reported formation of gahnite phase for Al concentrations higher than 1% by calcining the materials at 800°C. However, the lower calcination temperature used in the present investigation may justify the absence of secondary phases in the XRD diffractograms.

Increasing the Al content (Figure 5A) results in lower intensity of the ZnO patterns and therefore in the reduction of the mean particle size as summarized in Table 3. In fact, the mean particle size of ZnO (53.3 nm) becomes 49.5, 49.2, and 47.0 nm for 0.5% A-ZnO, 1.0% A-ZnO, and 1.5% A-ZnO, respectively. Consequently, the specific surface area, independently measured, increases from 4.2 $m^2 \cdot g^{-1}$ of bare ZnO to 11.5 $m^2 \cdot g^{-1}$. This may be explained because substitutional Al ions may be located in the grain frontiers of the ZnO particles, thus preventing their enlargement [41].

On the other hand, the crystallinity of the sample 1.0% A-ZnO increased with increasing calcination temperature (Figure 5B). Correspondingly, the mean particle size increased and the specific surface area decreased as summarized in Table 3. This effect is well known in literature for similar systems [42].

The substitution of Zn^{2+} with Al^{3+} ions is likely to occur due to the smaller ionic radius of Al^{3+} (0.039 nm) compared to Zn^{2+} (0.060) [43]. Ahmad et al. [23] reported that the presence of substitutional Al in the ZnO matrix leads to a decrease in the lattice parameters “a” and “c”. This hypothesis has been verified in the present system as shown in Figure 6, where the lattice parameters “a” and “c” have been calculated in function of the Al content.

Notably, only the variation of "a" and "c" have been considered as "b" is equal to "a" in the hexagonal structure.

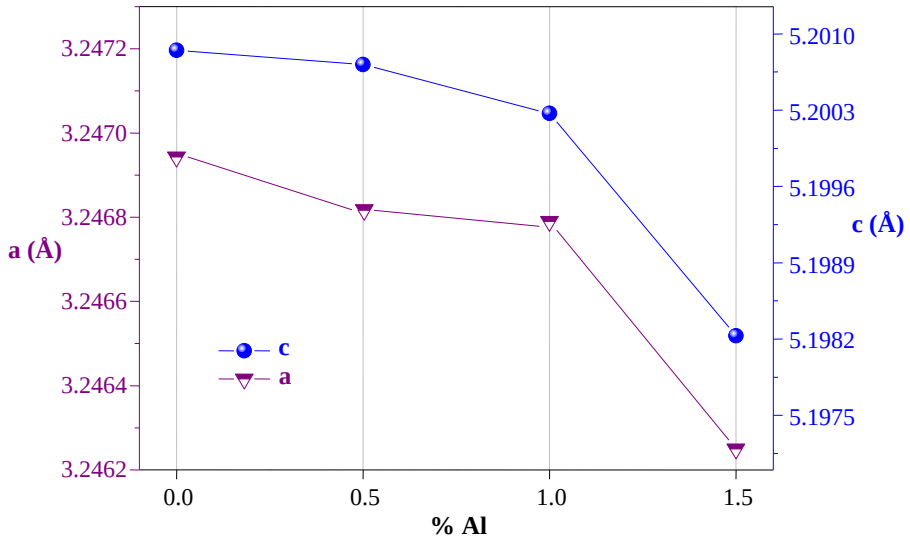

Figure 6. Variation of "a" and "c" lattice parameters with the aluminum content.

3.3.2 Raman spectroscopy analysis

Raman spectra of bare and Al doped ZnO samples are reported in Figure 7.

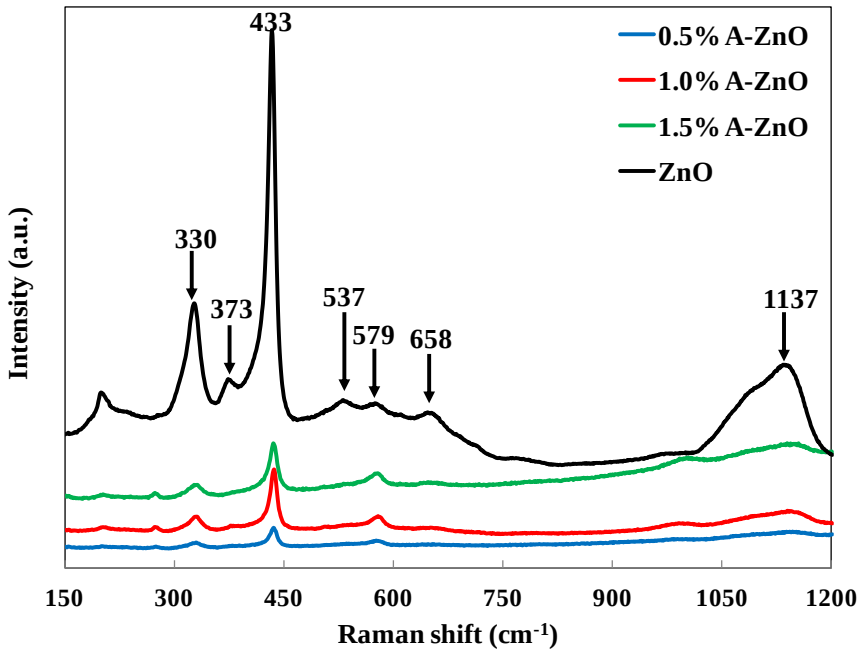

Figure 7. Raman spectra of bare and Al doped ZnO photocatalysts calcined at 600°C for 2h.

The Raman spectrum of pure ZnO presents bands ascribable to the wurtzite structure according to the relevant literature [44]. The intense peak at 433 cm^{-1} is assigned to the ZnO nonpolar optical phonon E_2(high) mode. The asymmetrical shape of this strong signal masks on its left side the E_1(TO) mode at 400 cm^{-1} generally associated with lattice disorder along the c-axis of the ZnO crystal. The peak at 330 cm^{-1} is ascribed to the A_1(LO) mode, while the peak at 373 cm^{-1} corresponds to the A_1(TO) mode. The peaks at 537, 658, and 1135 cm^{-1} are attributed to multiphonon scattering processes [44]. The peak at 579 cm^{-1} is attributed to the E_1(LO) mode, which is caused by defects such as oxygen vacancies, zinc interstitial, or other defects [45].

It is possible to observe that the relative intensity of almost all of the peaks, especially the one at 433 cm^{-1}, significantly decreased, while the bands at 330 and 579 cm^{-1} associated to LO modes, i.e. related to the defectivity, increased in the presence of Al in the ZnO matrix. These results, in agreement with the literature [46], indicate that Al doping changes the original hexagonal ZnO structure by reducing the crystal symmetry and introducing vacancies and substitutional defects which greatly affect the Zn-O stoichiometry.

3.3.3 FTIR analysis

Infrared spectra of the pure and Al modified ZnO samples are reported in Figure 8.

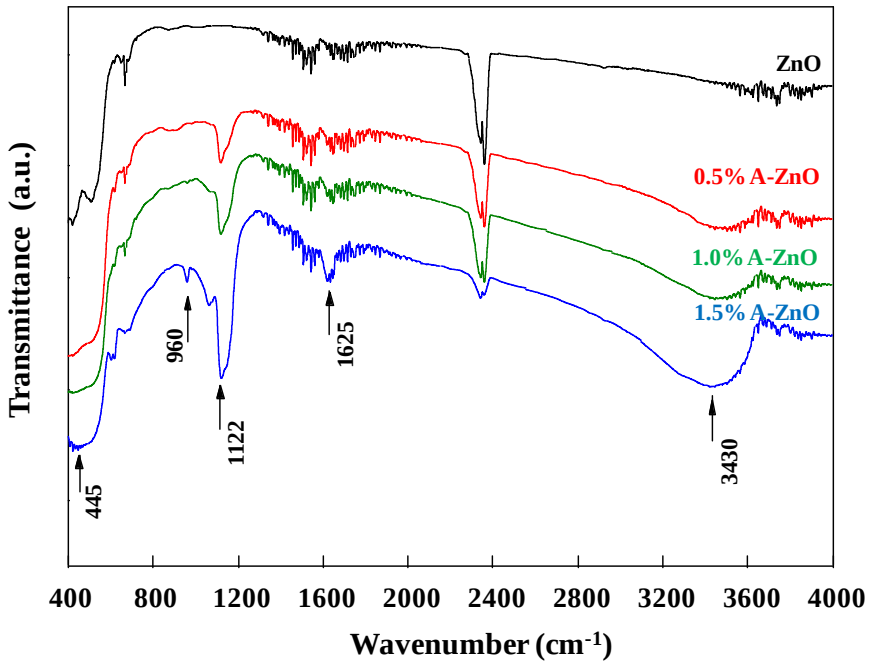

Figure 8. FTIR spectra of bare and Al doped ZnO photocatalysts calcined at 600°C for 2h.

The broad absorption band at 445 cm^{-1} is attributed to the Zn-O bond and it is obviously present in all of the spectra. The weak band at 960 cm^{-1} and the strong one at 1122 cm^{-1}, increasing in intensity with increasing Al content, are related to the stretching vibration of the Al-O bond [47], thus confirming the above mentioned (see XRD results) substitutional Al in the lattice of ZnO. The band at 2350 cm^{-1} is assigned to the bending vibration of atmospheric CO_2 molecules. The broad band at 3430 cm^{-1} and the weak band at 1625 cm^{-1}, particularly evident in the spectrum of the 1.5% A-ZnO sample, arise from the O-H vibration and H-O-H bending vibration, respectively, of adsorbed H_2O molecules.

It is possible to note that the intensity of the bands related to the presence of adsorbed water increases with increasing the Al content in the powder. This finding suggests that the presence of aluminum enhances the affinity of water with the surface. This may be due to the presence of the surface defects (detected by Raman spectroscopy) which may favor both the adsorption of IC and of water molecules. In fact, the surface Al^{+} ions arising from Al^{3+} insertion (see Eq. 3) may act as electron rich sites which easily interact with amphoteric compounds such as water. Notably, these findings justify both the results of photoactivity and

adsorption of IC in the dark. In the relevant literature the hydrophilicity of the surface has been often reported as a key parameter strongly affecting the activation energy [48], the dynamics of the charge carriers [49], the conversion and selectivity towards target compounds [50] of photocatalytic reactions. The higher affinity of the Al doped samples for water implies a higher degree of surface hydroxylation. The hydroxyl groups act both as (i) adsorption sites for the substrate and (ii) as traps for the photogenerated charges. Therefore, both the adsorption in the dark of the IC molecules and the photoactivity are improved with increasing the Al content up to the value of 1.0%. The subsequent reduction both in photoactivity and in dark adsorption observed for the 1.5% A-ZnO sample may be explained by considering that the water adsorption becomes so effective to hinder the adsorption of IC whose degradation efficiency thus decreases.

4. Conclusions

A simple sol-gel method has been used to synthesize Al doped ZnO samples with Al content ranging from 0 to 1.5%. The powders have been tested as photocatalysts for the degradation of a model compound (Indigo Carmine, IC) under UV light irradiation. Increasing the Al content of the doped samples resulted in higher ability of IC adsorption in the dark and superior photocatalytic activity for Al/Zn molar ratios up to 0.01 (1.0% A-ZnO sample). Higher Al contents provoked a reduction of both dark adsorption and photocatalytic efficiency. A thorough opto-electronic and structural characterization allowed to explain these findings. As far as the opto-electronic features are concerned, Al doping induced a blue shift of the band gap and a cathodic shift of the quasi Fermi level. However, as the extent of these modification was too low, it was concluded that the opto-electronic features did not play a significant role in the enhanced photocatalytic activity of the powders. On the other hand, the presence of surface defectivity induces high water affinity of the Al modified samples. In particular, the higher hydrophilicity of the doped samples increases the hydroxylation degree of the surface which results in (i) higher availability of active sites for the adsorption of the model compound, and (ii) higher generation rate of hydroxyl radicals during irradiation. These factors improve the photocatalytic activity until, at higher Al contents, water affinity is so high to compete with the substrate for adsorption thus hindering its degradation and decreasing the photocatalytic efficiency.

References

[1] V. Augugliaro, V. Loddo, G. Palmisano, M. Pagliaro and L. Palmisano, Clean by light irradiation: practical applications of supported TiO_2, RSC, Cambridge, 2010.

[2] G.B. Raupp, L.A. Dibble, Gas-solid photocatalytic oxidation of environmental pollutants, Patent n° CA2045517 C, 2002.

[3] F. Parrino, G. Camera-Roda, V. Loddo, G. Palmisano, V. Augugliaro, Combination of ozonation and photocatalysis for purification of aqueous effluents containing formic acid as probe pollutant and bromide ion, Water Res. 50 (2014) 189-199.

[4] P.V.L. Reddy, B. Kavitha, P.A.K. Reddy, K. Kim, TiO_2-based photocatalytic disinfection of microbes in aqueous media: A review, Environ. Res. 154 (2017) 296-303.

[5] P. Ragesh, V.A. Ganesh, S.V. Nair, A.S. Nair, A review on self-cleaning and multifunctional materials, J. Mater. Chem. A 2 (2014) 14773-14797.

[6] F. Parrino, A. Ramakrishnan, C. Damm, H. Kisch, Visible-light-induced sulfoxidation of alkanes in the presence of titania, ChemPlusChem 77 (2012) 713-720.

[7] C. Acar, I. Dincer, G.F. Naterer, Review of photocatalytic water-splitting methods for sustainable hydrogen production, Int. J. Energ. Res. 40 (2016) 1449–1473.

[8] A. Hagfeldt, G. Boschloo, L. Sun, L. Kloo, H. Pettersson, Dye-sensitized solar cells, Chem. Rev. 110 (2010) 6595–6663.

[9] C. Guarisco, G. Palmisano, G. Calogero, R. Ciriminna, G. Di Marco, V. Loddo, M. Pagliaro, F. Parrino, Visible-light driven oxidation of gaseous aliphatic alcohols to the corresponding carbonyls via TiO_2 sensitized by a perylene derivative, Environ. Sci. Pollut. Res. 21 (2014) 11135-11141.

[10] A. Abd-Elaal, F. Parrino, R. Ciriminna, V. Loddo, L. Palmisano and M. Pagliaro, Alcohol-selective oxidation in water under mild conditions via a novel approach to hybrid composite photocatalysts, ChemistryOpen 4 (2015) 779-785.

[11] G. Carini Jr., F. Parrino, G. Palmisano, G. Scandura, I. Citro, G. Calogero, A. Bartolotta, G. Di Marco, Nanostructured anatase TiO_2 densified at high pressure as advanced visible light photocatalysts, Photochem. Photobiol. Sci. 14 (2015) 1685-1693.

[12] M. Bellardita, H.A. El Nazer, V. Loddo, F. Parrino, A.M. Venezia, L. Palmisano, Photoactivity under visible light of metal loaded TiO_2 catalysts prepared by low frequency ultrasound treatment, Catal. Today 284 (2017) 92-99.

[13] W. Macyk, H. Kisch, Photosensitization of crystalline and amorphous titanium dioxide by Platinum(IV) chloride surface complexes, Chem. Eur. J. 7 (2001) 1862–1867.

[14] F. Parrino, E. García-López, G. Marcì, L. Palmisano, V. Felice, I. NataliSora, L.Armelao, Cu-substituted lanthanum ferrite perovskites: Preparation, characterization and photocatalytic activity in gas-solid regime under simulated solar light irradiation, J. All. Comp. 682 (2016) 686-694.

[15] G. Tan, L. Zhao, M.G. Kanatzidis, Rationally designing high-performance bulk thermoelectric materials, Chem. Rev. 116 (2016) 12123–12149.

[16] J. Jupille, G. Thornton, Defects at oxide surfaces, Springer, Switzerland, 2015.

[17] H. Cheng, X.J. Xu, H.H. Hng, J. Ma, Characterization of Al-doped ZnO thermoelectric materials prepared by RF plasma powder processing and hot press sintering, Ceram. Int. 35 (2009) 3067–3072.

[18] P. Zhang, R.Y. Honga, Q. Chen, W.G. Feng, On the electrical conductivity and photocatalytic activity of aluminium-doped zinc oxide, Powder Technol. 253 (2014) 360–367.

[19] K.C. Hsiao, S.C. Liao, Y.J. Chen, Synthesis, characterization and photocatalytic property of nanostructured Al-doped ZnO powders prepared by spray pyrolysis, Mater. Sci.and Eng. A 447 (2007) 71-76.

[20] M. Pal, S. Bera, S. Sarkar, S. Jana, Influence of Al doping on microstructural, optical and photocatalytic properties of sol–gel based nanostructured zinc oxide films on glass, RSC Adv. 4 (2014) 11552–11563.

[21] A. Alkahlout, N. Al Dahoudi, I. Grobelsek, M. Jilavi, P.W. de Oliveira, Synthesis and characterization of aluminum doped zinc oxide nanostructures via hydrothermal route, J. Mater. (2014) doi: 10.1155/2014/235638.

[22] S.D. Shinde, S.K. Date, A.V. Deshmukh, A. Das, P. Misra, L.M. Kukreja, K.P. Adhi, Role of Al doping in structural, microstructural, electrical and optical characteristics of as deposited and annealed ZnO thin films, RSC Adv. 5 (2015) 24178-24187.

[23] M. Ahmad, E. Ahmed, Y. Zhang, N.R. Khalid, J. Xu, M. Ullah, Z. Hong, Preparation of highly efficient Al-doped ZnO photocatalyst by combustion synthesis. Curr. Appl. Phys. 13 (2013) 697-704.

[24] J. Jia, A. Takasaki, N. Oka, Y. Shigesato, Experimental observation on the Fermi level shift in polycrystalline Al doped ZnO films, J. Appl. Phys. 112 (2012) doi: 10.1063/1.4733969.

[25] V. Devi, M. Kumar, D.K. Shukla, R.J. Choudhary, D.M. Phase, R. Kumar, B.C. Joshi, Structural, optical and electronic structure studies of Al doped ZnO thin films, Superlattices Microstruct. 83 (2015) 431–438.

[26] H.J. Lee, J.H. Kim, S.S. Park, S.S. Hong, G.D. Lee, Degradation kinetics for photocatalytic reaction of methyl orange over Al-doped ZnO nanoparticles, J. Ind. Eng. Chem. 25 (2015) 199–206.

[27] H. Kisch, On the Problem of Comparing Rates or Apparent Quantum Yields in Heterogeneous Photocatalysis, Angew. Chem. Inte. Ed., 49 (2010) 9588–9589.

[28] M. Rochkind, S. Pasternak, Y. Paz, Using dyes for evaluating photocatalytic properties: A critical review, Molecules 20 (2015) 88-110.

[29] X. Yan, T. Ohno, K. Nishijima, R. Abe, B. Ohtani, Is methylene blue an appropriate substrate for a photocatalytic activity test? A study with visible-light responsive titania, Chem. Phys. Lett. 429 (2006) 606-610.

[30] A. Hamrouni, N. Moussa, F. Parrino, A. Di Paola, A. Houas , L. Palmissano, Sol gel synthesis and photocatalytic activity of ZnO-SnO_2 nanocomposites, J. Mol. Catal. A :Chem. 390 (2014) 133-141.

[31] A. Hamrouni, N. Moussa, A. Di Paola, F. Parrino, A. Houas, L. Palmisano, Characterization and photoactivity of coupled ZnO–$ZnWO_4$ catalysts prepared by a sol–gel method, Appl. Catal. B: Environ. 154–155 (2014) 379–385.

[32] A. Hamrouni, N. Moussa, A. Di Paola, L. Palmisano, A. Houas, F. Parrino, Photocatalytic activity of binary and ternary SnO_2-ZnO-$ZnWO_4$ nanocomposites, J. Photochem. Photobiol. A 309 (2015) 47-54.

[33] H. Lachheb, F. Ajala, A. Hamrouni, A. Houas, F. Parrino, L. Palmisano, Electron transfer in ZnO–Fe_2O_3 aqueous slurry systems and its effects on visible light photocatalytic activity, Catal. Sci. Technol. (2017) doi: 10.1039/C7CY01085K.

[34] A.M. Roy, G.C. De, N. Sasmal, S.S. Bhattachayya, Determination of the flatband potential of semiconductor particles in suspension by photovoltage mesurement, Int. J. Hydrogen Energy 20 (1995) 627– 630.

[35] P. Wardman, Reduction potentials of one-electron couples involving free radicals in aqueous solution, J. Phys. Chem. Ref. Data, 18 (1989) 1637-1755.

[36] P. Granger, V.I. Parvulescu, S. Kaliaguine, W. Prellier, Perovskites and related mixed oxides: Concepts and applications Vol. 1, Wiley, 2016.

[37] A.V. Singh, R.M. Mehra, A. Yoshida, A. Wakahara, Doping mechanism in aluminum doped zinc oxide films. J. Appl. Phys. 95 (2004) 3640-3643.

[38] M. Grundmann, The physics of semiconductors, Springer, Berlin Heidelberg New York, 2006.

[39] T. Gupta, Microstructural engineering through donor and acceptor doping in the grain and grain boundary of a polycrystalline semiconducting ceramic, J. Mater. Res. 7 (1992) 3280-3295.

[40] T. Tsubota, M. Ohtaki, K. Eguchi, K. Arai, Thermoelectric properties of Al-doped ZnO as a promising oxide material for high temperature thermoelectric conversion. J. Mater. Chem. 7 (1997) 85-90.

[41] W.S. Hong, L.C. De Jonghe, X. Yang, M.N. Rahaman, Reaction sintering of ZnO-Al_2O_3, J. Am. Ceram. Soc. 78 (1995) 3217-3224.

[42] A.K. Pandeya, K. Biswas, Effect of agglomeration and calcination temperature on the mechanical properties of yttria stabilized zirconia (YSZ), Ceram. Int., 40 (2014) 14111–14117.

[43] D.R. Lide, Ionic radii in crystals, in CRC handbook of Chemistry and physics, eds. W.M. Haynes and D.R. Lide, CRC Press/Taylor and Francis, Boca Raton, FL, 2012.

[44] J.M. Calleja, M. Cardona, Resonant Raman scattering in ZnO, Phys. Rev. B 16 (1977) 3753–3761.

[45] A.K. Pradhan, K. Zhang, G.B. Loutts, U.N. Roy, Y. Cui, A. Burger, Structural and spectroscopic characteristics of ZnO and ZnO:Er^{3+} nanostructures, J. Phys. Condens. Matter 16 (2004) 7123–7129.

[46] A. El Manouni, F.J. Manjón, M. Mollar, B. Marí, R. Gómez, M.C. López, J.R. Ramos-Barrado, Effect of aluminum doping on zinc oxide thin films grown by spray pyrolysis Superlattices Microstruct. 39 (2006) 185-192.

[47] W.T. Kaltchev, M. Tysoe, An infrared spectroscopic investigation of thin alumina films: measurement of acid sites and surface reactivity, Surf. Sci. 430 (1999) 29–36.

[48] F. Parrino , P. Conte, C. De Pasquale, V.A. Laudicina, V. Loddo, L. Palmisano, Influence of adsorbed water on the activation energy of model photocatalytic reactions, J. Phys. Chem. C 121 (2017) 2258–2267.

[49] A. Litke, Y. Su, I. Tranca, T. Weber, E.J.M. Hensen, J.P. Hofmann, Role of adsorbed water on charge carrier dynamics in photoexcited TiO_2, J. Phys. Chem. C: Nanomater. Interfaces 121 (2017) 7514–7524.

[50] J. Kou, C. Lu, J. Wang, Y. Chen, Z. Xu, R.S. Varma, Selectivity enhancement in heterogeneous photocatalytic transformations, Chem. Rev. 117 (2017) 1445–1514.